Protein polymer nanoparticles engineered as chaperones protect against apoptosis in human retinal pigment epithelial cells

Wan Wang[#1], **Parameswaran G Sreekumar**[#2], **Vinod Valluripalli**[1], **Pu Shi**[1], **Jiawei Wang**[1], **Yi-An Lin**[6], **Honggang Cui**[6], **Ram Kannan**[2], **David R Hinton**[3,4], and **J. Andrew MacKay**[1,5]

[1]Department of Pharmacology and Pharmaceutical Sciences, University of Southern California Los Angeles, CA; 90033-9121

[2]Arnold and Mabel Beckman Macular Research Center, Doheny Eye Institute, Los Angeles, CA 90033

[3]Department of Ophthalmology, Keck School of Medicine of the University of Southern California, Los Angeles, CA 90033

[4]Department of Pathology, Keck School of Medicine of the University of Southern California, Los Angeles, CA 90033

[5]Department of Biomedical Engineering, University of Southern California, Los Angeles, CA 90033

[6]Department of Chemical and Biomolecular Engineering, Johns Hopkins University, Baltimore, 21218, USA

[#] These authors contributed equally to this work.

Abstract

αB-crystallin is a protein chaperone with anti-apoptotic and anti-inflammatory activity that is apically secreted in exosomes by polarized human retinal pigment epithelium. A 20 amino acid mini-peptide derived from residues 73-92 of αB-crystallin protects human retinal pigment epithelial (RPE) cells from oxidative stress, a process involved in the progression of age related macular degeneration (AMD). Unfortunately, due to its small size, its development as a therapeutic requires a robust controlled release system. To achieve this goal, the αB-crystallin peptide was re-engineered into a protein polymer nanoparticle/macromolecule with the purpose of increasing the hydrodynamic radius/molecular weight and enhancing potency via multivalency or an extended retention time. The peptide was recombinantly fused with two high molecular weight (~40 kD) protein polymers inspired by human tropoelastin. These elastin-like-polypeptides (ELPs)

Corresponding author: MacKay, J. Andrew (jamackay@usc.edu) **Address:** Department of Pharmacology and Pharmaceutical Sciences, University of Southern California; Los Angeles, CA; 90033-9121. Phone Number: 323-442-4118.

include: i) a soluble peptide called S96; and ii) a diblock copolymer called SI that assembles multivalent nanoparticles at physiological temperature. Fusion proteins, cryS96 and crySI, were found to reduce aggregation of alcohol dehydrogenase and insulin, which demonstrates that ELP fusion did not diminish chaperone activity. Next their interaction with RPE cells was evaluated under oxidative stress. Unexpectedly, H_2O_2-induced stress dramatically enhanced cellular uptake and nuclear localization of both cryS96 and crySI ELPs. Accompanying uptake, both fusion proteins protected RPE cells from apoptosis, as indicated by reduced caspase 3 activation and TUNEL staining. This study demonstrates the *in vitro* feasibility of modulating the hydrodynamic radius for small peptide chaperones by seamless fusion with protein polymers; furthermore, they may have therapeutic applications in diseases associated with oxidative stress, such as AMD.

Keywords

Elastin-like polypeptide (ELPs); assembly; chaperone; anti-apoptosis; cell uptake

1. Introduction

Small heat-shock proteins (sHSPs) maintain protein homeostasis by binding substrate proteins in non-native conformations and preventing irreversible aggregation [1]. Partly mediated by oligomerization, they shift between an inactive low-affinity state and active high-affinity oligomers. Stress, such as heat shock, shifts their equilibrium towards formation of active oligomers. By forming intermediate complexes with nonnative protein conformations, these active oligomers guard against protein denaturation [1]. One member of the sHSPs family, αB-crystallin has attracted attention due to its roles in neuroprotection, anti-inflammation, and biophysics of assembly [2]. Ongoing research by our group has focused on its potential for treating age-related macular degeneration (AMD) via protection against apoptosis induced by oxidative stress [3]. It has been reported that αB-crystallin expression increases in retinal pigment epithelial (RPE) cells of patients with both late 'dry' and 'wet' AMD [4]. We reported that prominent expression of αB-crystallin correlates with the observation of drusen, which are extracellular subretinal deposits associated with early AMD [5]. In RPE cells, αB-crystallin has significant cytoprotective effects mediated by suppression of protein aggregation and the proteolytic action of caspase 3 [3].

αB-crystallin is composed of a conserved α-crystallin domain flanked by a variable N-terminal domain and a C-terminal extension. Similar to other sHSPs, the α-crystallin domain consists of 6-8 β-strands organized in two β-sheets [6]. Surprisingly, Bhattacharyya and coworkers reported that residues 73–92 of αB-crystallin (DRFSVNLDVKHFSPEELKVK) are sufficient to prevent aggregation of denatured substrate proteins *in vitro,* similar to the full length protein [7]. The fact that this 'mini-peptide' retains full chaperone activity suggests that it too has therapeutic potential to rescue RPE cells from oxidative stress. In contrast, an overlapping (underlined amino acids) fragment of residues 90-100 of αB-crystallin (KVKVLGDVIEV) forms oligomeric fibrils exhibiting β-sheet–rich structures similar to other amyloid oligomers [8]. These oligomers exhibit cytotoxicity and can be recognized by an oligomer-specific antibody [8]. Thus, overlapping short peptides from αB-crystallin appear to have diametrically opposing effects on cell viability. Although the

correlation between mini-αB-crystallin's oligomeric flexibility and its cytoprotective/ cytotoxic role is less clear, one postulation is that the peptide's quaternary dynamics [9] underlie its chaperone function both *in vitro* and in the crowded cellular environment. Unfortunately, as a small peptide, the residence time near the retina following either systemic or intravitreal administration is expected to be short [10-13]. For this reason, we are exploring simple approaches to engineer the mini-peptide (residues 73-92) onto a high molecular weight carrier that has the potential to modulate local and systemic residence time, potentiate binding and internalization, and enhance protection from oxidative stress.

An emerging method to bioengineer peptides with potent biological activity is to fuse them to protein polymers. Protein polymers can provide a platform for controlling release, multivalency, molecular weight, phase behavior, and even nanoparticle assembly [14-17]. One class of protein polymers known as elastin-like polypeptides (ELPs) are composed of the repetitive pentapeptide motif (Val-Pro-Gly-Xaa-Gly)$_n$ [18]. ELPs have unique reversible inverse phase transition temperatures, T_t, below which they solubilize and above which they phase separate. T_t can be tuned through selection of guest residue identity (Xaa) and the number of pentameric repeats, *n*. ELP fusion proteins are being evaluated for effects due to their hydrodynamic radius, self-assembly of nanoparticles, or formation of thermo responsive deposits in multiple disease models [19-21]. Prior to this report, no studies of protein polymers have explored; i) their fusion with chaperone proteins; ii) their ability to modify oligomerization of peptide fibrils; or iii) their intracellular behavior under oxidative stress, all to which are relevant to the treatment of AMD.

Herein, we report the rational bioengineering of the 'mini-peptide' from αB-crystallin into two types of ELP fusion proteins (Table 1). crySI has been engineered onto a nanoparticle ELP scaffold called SI (Fig. 1). For comparison, the peptide has also been fused to a soluble ELP of similar molecular weight called cryS96. Similar to their parent ELPs, the fusion constructs have temperature-dependent assembly that interrupted the native oligomerization of cry peptide as confirmed by TEM and DLS. Similar to the free 'mini-peptide', the ELP fusion proteins inhibit the aggregation of substrate proteins, including alcohol dehydrogenase (ADH) and insulin. Furthermore, exogenous cryELPs also protect RPE cells against hydrogen peroxide (H_2O_2) induced apoptosis and undergo nuclear translocation in RPE cells under H_2O_2 stress. Interestingly, cryS96 exhibited better protection against apoptosis than the free cry peptide at the same molar concentration.

2. Materials and Methods

2.1 Materials and reagents

TB DRY® Powder Growth Media was purchased from MO BIO Laboratories, Inc. (Carlsbad, CA). NHSRhodamine was purchased from Thermo Fisher Scientific (Rockford, IL). Alcohol dehydrogenase (ADH) and Insulin were purchased from Sigma-Aldrich (St. Louis, MO). αB-crystallin mini-chaperone (cry, DRFSVNLDVKHFSPEELKVK) and a scrambled peptide control (Neg, DLPLKKNVEDKFHRSFVESV) were synthesized by Neo-peptide (Cambridge, MA). Anti-LAMP1 antibody was purchased from Abcam and Monodansylcadaverine (MDC) was obtained from Sigma. The protocol for the preparation and use of cultured human fetal RPE cells were approved by the University of Southern

California Institutional Review Board under protocol #HS-947005 and adhered to the tenets of the Declaration of Helsinki. RPE cells were isolated from human fetal eyes (gestational age 16–18 weeks) obtained from Advanced Bioscience Resources, Inc. (ABR, Alameda, CA). Primary cultures of RPE cells were established as described previously [22] and used at passages 3 to 4.

2.2 Construction of ELP genes

Genes encoding for ELPs (S96 and SI) were synthesized by recursive directional ligation in pET25b(+) vector as previous reported [20]. Sense and antisense DNA oligonucleotides encoding for the mini-peptide were synthesized with NdeI (5') and BamHI (3') overhangs were synthesized at University of Southern California DNA core facility. Forward sequence: 5'-TATGGGTGATAGATTTAGCGTTAACCTGGACGTGAAACATTTCTCCCCAGAAGA ACTGAAAGTGAA GGGTTATTAGACTCCTCG-3'. Reverse sequence: 5'-ATCCGAGGAGTCTAATAACCCTTCACTTTCAGTTCTTCTGGGGGAGAAATGTTTCA CGTCCAGGTTA ACGCTAAATCTATCACCCA-3'. Complementary oligonucleotides were heated at 95°C for 5 minutes and annealed at room temperature for 2h. Annealed oligos were inserted into pET25b(+) vector, digested with NdeI and BamHI. A BseRI recognition site was also incorporated to facilitate the insertion of ELP genes. Correct ligation of the fusion protein gene was confirmed by restriction digestion and DNA sequencing. Sequences were confirmed by DNA sequencing in the core facility of the Norris Cancer Center of the University of Southern California.

2.3 ELP expression and purification

ELPs (Table 1) were expressed in BLR (DE3) *E. coli* competent cells (Novagen Inc., Milwaukee, WI). Cells were inoculated in ampicillin medium and grown for 24 h at 37 °C. The bacterial culture was centrifuged, disrupted by probe-tip sonicated in ice cold PBS and centrifuged to remove insoluble cell debris. ELPs were purified from the cell supernatant by inverse transition cycling (ITC) [23]. Purity of ELP fusion proteins was determined by SDS-PAGE gels stained with coomassie blue. Protein concentrations were determined by UV-visible spectroscopy of the carboxy terminal tyrosine at 280 nm ($\varepsilon=1285 M^{-1}cm^{-1}$). Protein molecular weight was further confirmed by MALDI-TOF analysis.

2.4 Transmission Electron Microscopy (TEM) imaging

The TEM imaging was carried out on a FEI Tecnai 12 TWIN microscope (Hillsboro, OR) at 100 kV. The samples were prepared by using the following protocol: A 100 μM solution (5 μL) was initially deposited on a copper grid with carbon film (CF400-Cu, Election Microscopy Sciences, Hatfield, PA). Excess amount of the solution was removed by filter paper. The samples were then negatively stained with 2% uranyl acetate, and the excess uranyl acetate solution was removed by filter paper after 30 seconds. The samples were dried under room temperature for at least 3 hours before they were used for imaging.

2.5 Characterization of ELP particle formation and phase transition temperature

The temperature-concentration phase diagrams for ELP fusion proteins were characterized by optical density, and the self-assembly of nanoparticles was confirmed using dynamic light scattering (DLS). Optical density was recorded using a DU800 UV-Vis spectrophotometer at 350 nm as a function of solution temperature. Typically, ELPs (5 – 100 μM) were heated at 1 °C/min from 10 to 85 °C and sampled every 0.3 °C. T_t was defined at the point of the maximum first derivative. Similarly, hydrodynamic radius (Rh) was recorded to characterize particle size distribution as a function of temperature. Briefly, protein samples were prepared at 25 μM in PBS and filtered through a 20 nm filter at 4 °C. Autocorrelation functions were collected u sing a DynaPro-LSR Plate Reader (Wyatt Technology, Santa Barbara, CA). Light scattering data were collected at regular temperature intervals (1 °C) as solutions were heated from 5 to 60 °C. Th e results were analyzed using a Rayleigh sphere model and fitted into either a regularization or cumulant algorithm based on the sum-of-squares value. The critical micelle temperature (CMT) for each protein construct was defined as the lowest temperature at which the R_h is significantly greater than the average monomer R_h.

2.6 Bis-ANS assay

The hydrophobicity of cryELPs was evaluated using fluorescent probe 1,1*-bi(4 anilino)naphthalenesulfonic acid (bis-ANS) on a HORIBA Jobin Yvon Fluorolog-3 Spectrofluorometer. bis-ANS (Sigma-Aldrich) stock solution was prepared in 95% alcohol and the concentration was determined by absorbance at 385 nm ($\varepsilon_{385} = 16,790\ cm^- M^-$). Samples with 5 μM bis-ANS were excited at 390 nm, and the emission spectra were then recorded at 400-600 nm. The excitation and emission slits were set at 5 nm.

2.7 Quantification of chaperone activity

Chaperone activity was measured using two protein substrates: ADH and insulin [7]. The kinetics of aggregation was monitored by optical density at 360 nm with a Beckman DU800 UV-Vis spectrophotometer equipped with a temperature-controlled multi-cell transporter. Assays were done in the absence or presence of ELP fusion peptides. Aggregation of ADH (100 μg /300 μl) was monitored upon incubation at 48 °C at a molar ratio of ADH to peptide of 1:250. For insulin aggregation, 120 μg/300 μl insulin (bovine pancreas) were induced to aggregate by addition of 80 mM Dithiothreitol (DTT) at 12 °C at a molar ratio of insulin to pepti de of 0.7:1. Heat capacity measurements were performed using a Perkin Elmer Differential Scanning Calorimeter (DSC) 8500.

2.8 NHS-Rhodamine labeling of recombinant ELP fusions

For fluorescent visualization, ELPs were covalently modified with NHS-Rhodamine (Thermo Fisher Scientific Inc, Rockford, IL) via the primary amino terminus. Briefly, the conjugation was performed in 100 mM borate buffer (pH 8.5) overnight at 4 °C. E xcess fluorophore was removed using a desalting PD-10 column (GE Healthcare, Piscataway, NJ) and overnight dialysis against PBS at 4 °C.

2.9 Protection of RPE cells from H₂O₂ induced cell death

The anti-apoptotic effects of crySI and cryS96 were studied by TUNEL staining and western blot detection of caspase 3 activation in confluent human RPE cells upon challenge with H_2O_2. Briefly, human RPE cells grown on 4-well chamber slides were starved overnight in FBS free medium and treated with 200 μM H_2O_2 for an additional 24 h. For TUNEL staining, cell death was assessed by terminal deoxynucleotidyl transferase dUTP nick end labeling (TUNEL) following the manufacturer's protocol (Roche, IN). After treatment RPE cells were washed in PBS, air dried, and fixed with freshly prepared 4 % paraformaldehyde. Cells were permeabilized with Triton X-100 and incubated with the TUNEL reaction mixture for 1 h in the dark at 37 °C . Cells were washed, stained with 4',6-diamidino-2-phenylindole (DAPI) and viewed under a spinning disc laser scanning confocal microscope (PerkinElmer, MA). TUNEL positive cells were counted and quantified as described [3]. For immunoblot analysis, protein was extracted from the RPE cells at the end of indicated experiments. Equal amounts of protein (60 μg) were resolved on 15 % Tris-HCl polyacrylamide gels. Membranes were probed with rabbit polyclonal anti-cleaved caspase-3 antibody (1:1000, Cell Signaling, MA). After incubation with the corresponding secondary antibodies, signals were detected using a chemiluminescence system. GAPDH was used as a loading control.

2.10 Intracellular uptake in RPE cells under H₂O₂ induced stress

Confluent human RPE cells cultured on 4 well chamber slides were co-incubated with 200 μM H_2O_2 and 5 μM rhodamine labeled ELPs or cry peptide for indicated time periods. For immunofluorescence, the cells after the experiments were fixed in 4 % paraformaldehyde for 20 min, followed by permeabilization with 0.1 % triton-X for 15 min. Cells were blocked with 5 % goat serum and incubated with LAMP-1 (1:100) over night at 4 °C. After wash ing the cells were incubated with FITC labeled secondary antibody for 30 min at RT, cells were mounted with DAPI and observed under a LSM 510 confocal microscope (Zeiss).

2.11 Statistical analysis

Data presented are representative curves or mean ± S.D. All experiments were repeated at least three times. Statistical analysis was performed by Student t-test, one-way or two-way ANOVA by GraphPad Prism 5.01. Differences between treatments were established with Tukey's or Bonferroni's post-hoc test. A p value of less than 0.05 was considered statistically significant.

3 Results

3.1 Purification of ELP fusion proteins that assemble nanoparticles

To investigate the potential for assembling protein polymers with chaperone activity, ELP genes with and without the chaperone mini-peptide from αB-crystallin were cloned into a pET25b(+) vector (Table 1), expressed in *E. coli* cells, and purified using Inverse Transition Cycling (ITC) as previously reported [24, 25]. After purification all four protein polymers yielded between 30-40 mg/L culture. Purified proteins were confirmed to have the correct molecular weight and high purity when assessed using SDS PAGE (Fig. 1A). MALDITOF

was used to reconfirm that all proteins purified were within 1.5 % of their expected molecular weight (Table 1). The ELPs resulting from a diblock copolymer, SI and crySI were assessed for nanoparticle morphology using TEM (Fig. 1B). The dominant species observed for both SI and crySI formulations were spherical nanoparticles with diameters of 29.1 ± 3.4 nm and 28.7 ± 6.2 nm respectively. Using TEM, the free cry peptide was confirmed to mediate the formation of oligomers and fibers; furthermore, fibril formation was disrupted by scrambling the amino acid sequence (Supplementary Fig. S1). Interestingly, cryS96 did not form either fibril or oligomer structures (Supplementary Fig. S1), which suggests that the ELP fusion may sterically interfere with the oligomerization of the native cry peptide.

3.2. The mini-peptide from αB-crystallin shifts the phase diagram for ELP nanoparticles

To characterize a concentration-temperature phase diagram for the ELP fusions, optical density was monitored as a function of temperature to identify relevant transition temperatures (T_{t1}, T_{t2}) (Fig. 2). SI exhibited a steep thermal response at 26 °C, T_{t1}, which correlates with the phase transition temperature of the more hydrophobic (Xaa=Ile) block. This lower transition temperature can be defined as the critical micelle temperature [20]. At a higher temperature, T_{t2}, near 75 °C, the more hydrophilic block (Xaa=Ser) collapses and SI undergoes bulk phase separation (Fig. 2A). Similar to SI, crySI shows two obvious phase transitions, where T_{t1}, T_{t2} are 13, 30 °C respectively. In comparison to SI, the mini-peptide on crySI has the effect of depressing both transition temperatures across the experimental concentration range (Fig. 2B). On the contrary, both S96 and cryS96 exhibit only one T_t near 55 °C, which was unchanged by addition of the mini-peptide (Fig. 2C,D). Most notably, concentration dependence of T_{t1} for crySI (-0.4 ± 0.6 °C / Log$_{10}$[μM]) was significantly suppressed compared to SI (-22.6 ± 16.0 °C / Log$_{10}$[μM]) as fit with a log-linear regression line (mean slope ± 95% confidence interval) Despite this impact on the phase diagram, crySI still forms a population of relatively monodisperse nanoparticles of a similar diameter to SI at room temperature (Fig. 1C).

Due to the shift in the concentration-temperature phase diagram induced by fusion with the mini-peptide, dynamic light scattering (DLS) was used to determine what species exist above and below the boundaries identified by optical density (Fig. 2). Two fitting models were used to interpret the DLS autocorrelation functions. First a cumulant fit was performed, which assumes the existence of only a single population of particles. This robust approach was adequate for fitting both SI and S96 (Fig. 3A,D); however, fusion of the mini-peptide to either polymer resulted in a scattering dominated by a particle of larger dimensions (Fig. 3B,E). Since SI and S96 do not assemble structures until above 25 and 60 °C respectively, the data suggest that the m ini-peptide alone mediates nanoparticle assembly. Assuming that a smaller population of free crySI and cryS96 exist in equilibrium with a larger assembled population, a second model called regularization was used to interrogate the data (Fig. 3C,F). Regularization corrects for the relative difference in scattering intensity from mixtures of particles with different hydrodynamic radii. Using the regularization model, SI and S96 continued to behave as single population of particles. This was not the case for crySI and cryS96, which were fit best at the lowest temperatures as a mixture of a small (4 to 5 nm) and large (30 to 40 nm) population of particles, where the smaller population

represents more than 95% of the polymer mass in solution (Fig. 3C,F). For cryS96, this distribution was roughly constant over the entire temperature range (Fig. 3F). This suggests that even in the absence of ELP-mediated assembly, the mini-peptide mediates relatively weak assembly of nanoparticles. For crySI, regularization fitting identified two particle populations over the observed temperature range. As observed using optical density (Fig. 2B), crySI undergoes two thermally-induced changes in the distribution of hydrodynamic radii. Below 13 °C, the smaller population of crySI particles accounts for the majority of the sample monomers, which was similar to cryS96. Between 13 and 26 °C crySI increases in opt ical density (Fig. 2B), and the resulting mixture could not be fit by either the cumulant or regularization models (Fig. 3B,C). There was a narrow intermediate window (26 to 28 °C) where crySI was d ominated (100% by mass) by nanoparticles similar to SI. Above 30 °C, crySI nanoparticles pro ceeded to assemble into larger nanoparticles (300 to 500 nm), which dominated the sample (99% by mass). Above 30 °C, a small fraction of the sample remained in nanoparticles similar to SI; however, this represents only 1% of the mass of the sample. Thus, both crySI and cryS96 have thermal assembly properties similar to their unmodified ELP; however, the mini-peptide significantly impacts the distribution of particle sizes.

3.4 crySI and cryS96 behave as molecular chaperones

Substrate proteins alcohol dehydrogenase (ADH) and insulin were used to test chaperone activity of ELPs with and without the αB-crystallin mini-peptide. Chaperone activity against ADH was characterized at 48 °C (Fig. 4A,B). Both the mini-p eptide alone and cryS96 inhibited ADH aggregation in a concentration dependent manner, with an IC_{50} of 260 ± 99 μM and 205 ± 29 μM (Supplementary Fig. S2). To confirm the importance of the mini-peptide sequence, a scrambled mini-peptide (Neg) was also evaluated and showed no chaperone activity. Due to the confounding optical densities of SI and crySI at 48 °C (Fig. 2B), heat induced ADH aggregat ion was inconclusive and is not shown. To further investigate the mechanism of chaperone activity, differential scanning calorimetry was used to determine the enthalpy of ADH aggregation in the presence and absence of cryS96 (Fig. 4C). This study revealed that cryS96 reduced the specific enthalpy of ADH aggregation, while the ELP alone did not (Fig. 4C). To compare the relative chaperone activity of crySI and cryS96, an insulin chaperone assay was performed at 12 °C upon the addition of D TT (Fig. 4D,E). At 30 minutes, both crySI and cryS96 suppressed more optical density compared to controls SI and S96 (p<0.001). Noticeably, crySI inhibited insulin aggregation by $64.6 \pm 5.4\%$, which was greater than the protective effect of cryS96 ($50.9 \pm 4.2\%$) (p<0.05) (Fig. 4D,E). Control ELPs SI and S96 as well as the scrambled peptide Neg lacked any chaperone activity towards insulin.

Protein chaperones protect RPE cells against apoptosis by interfering with caspase activation and/or mitochondrial processes that lead to cell death [26]. Having demonstrated that crySI and cryS96 both have chaperone activity, their potential anti-apoptotic properties were evaluated on RPE cells co-incubated with 200 μM H_2O_2 for 24 hours. To quantify apoptosis, the TUNEL assay was used to identify apoptotic cells, which showed around 20 % cell death. Similar to the free cry peptide, crySI and cryS96 treatment significantly reduced cell death (p<0.05) compared to unmodified ELP controls (Fig. 5A,B). Unmodified ELPs did not produce apoptosis in RPE; however, co-incubation of plain ELP with H_2O_2 resulted in cell

death. To confirm that the TUNEL assay was detecting apoptosis, caspase 3 activation was also characterized using a western blot. Activation of caspase 3 in RPE was reduced in cryS96 and crySI compared to ELPs alone (Fig. 5C). Collectively, results from the TUNEL and caspase 3 activation assays demonstrate that only the ELPs with the cry peptide activity exhibit anti-apoptotic properties, and both crySI and cryS96 inhibited caspase 3 activation to a similar degree.

3.6 Cell uptake and nuclear localization of crySI and cryS96 under oxidative stress is important for anti-apoptosis activity

We have previously shown that exogenous recombinant αB crystallin and the mini-αB crystallin peptide (cry) can be taken up by RPE cells [26], which may play a role in the suppression of apoptosis. To determine if exogenous ELP fusions to the mini-peptide would also have access to the cytosol, confocal microscopy was used to track the internalization of rhodamine labeled material. In addition to incubation with 5 μM of labeled ELPs, cells were also observed in the absence and presence of oxidative stress from H_2O_2 (200 μM for 24 h). All ELPs showed evidence of punctate intracellular accumulation in the cytoplasm; however, to our surprise oxidative stress significantly induced nuclear localization of SI, crySI, and cryS96 (Fig. 6). crySI exhibited higher cell uptake than cryS96 ($p<0.001$).

Based on the combined observations that both cryS96 and crySI are protective against apoptosis (Fig. 5) and translocate to the nucleus under oxidative stress (Fig. 6), we next investigated whether uptake was necessary for protection and dependent on endocytosis. Since both cryS96 and crySI provide the same degree of apoptotic protection, chaperone activity, and nuclear translocation, cryS96 alone was subsequently characterized for its mechanism of internalization (Fig. 7). We hypothesized that if cryS96 internalizes by clathrin-mediated endocytosis, then inhibitors of this pathway should both block nuclear translocation and also abolish the anti-apoptosis activity. Monodansylcadaverine (MDC) blocks clathrin-mediated endocytosis; furthermore, it efficiently halted the nuclear translocation of cryS96 under oxidative stress (Fig. 7A). A similar effect was observed when cells were treated with Dynasore, which blocks dynamin-dependent internalization (Supplementary Fig. S3). Remarkably, inhibition of cryS96 endocytosis completely eliminated protection against TUNEL positive cells under oxidative stress (Fig. 7B,C).

Based on the evidence that cryS96's anti-apoptotic activity depends on cellular uptake, we further hypothesized that the exogenous chaperone must partially escape from the classical endosomelysosome pathway in order to reach its intracellular targets. We thus used the late endosome/lysosome marker LAMP1 to track localization of cryS96 and cry peptide inside RPE cells at early time points (Fig. 8). Surprisingly, at 1h most cryS96 exhibited nuclear translocation while a significant amount of free cry peptide was retained in the cytosol and partially colocalized with LAMP1. At 4 h, both cryS96 and cry peptide had translocated to the nucleus and no longer showed co-localization with LAMP 1. This study thus suggests that both the cry peptide alone and cryS96 bypass the endo-lysosomal compartment of human RPE cells under oxidative stress. This access to the cytosol results later in their translocation to the nucleus (Fig. 6) and correlates with their anti-apoptotic effect (Fig. 5,7).

4 Discussion

Age-related macular degeneration (AMD) is the leading cause of blindness among older individuals in the western world, with more than 13 million cases per year in the United States alone [27]. Currently there is no effective therapy for dry AMD; however, we and others have proposed that exogenous sHSPs may be developed as therapeutics for AMD [28, 29]. The immunomodulatory and anti-apoptotic function of molecular chaperones should be an important consideration in the development of therapeutic interventions due to their ability to enhance cell viability under deleterious conditions including oxidative stress [30, 31]. As successful examples, Ousman et al. have demonstrated the negative regulatory role of αB-crystallin on several inflammatory pathways in the immune and central nervous systems [32]; Rothbard and co-workers have illustrated the therapeutic effects of αB-crystallin associated with specific proinflammatory plasma protein binding via systemic administration [33]. Moreover, Arac et al. have described effective treatment of experimental stroke using αB-crystallin even twelve hours post-stroke onset [34]. Herein, we intended to utilize the intermolecular association/dissociation of a mini-peptide derived from αB-crystallin [35, 36], explore its thermal and chaperone activities in fusion with ELPs (Fig. 1), and evaluate the fusion protein's cell-protective and uptake properties under oxidative stress in a human RPE model. The resulting fusions may have applications as therapeutic chaperones for AMD.

A prevalent view regarding the mechanism of action for sHSPs is that they interact with exposed hydrophobic patches on client proteins undergoing aggregation [9]. Previous studies indicated that exposure of hydrophobic surface change and reorganization of oligomer architecture are associated with αB-crystallin's chaperone function [37-39]. TEM images of all peptides and fusion proteins involved in the study provided the first clue of ELPs' modulation of native cry peptide assembly (Fig. 1 & S1). To gain more insight into the hydrophobicity change of cry peptide by fusion with ELPs, we analyzed the temperature dependent hydrophobicity of cry, crySI and cryS96 via Bis-ANS assay [7] (Supplemental Fig. S4). Noticeably, only crySI exhibited a significant temperature triggered hydrophobicity change (****$p<0.0001$), which was consistent with its observed stepwise aggregation via DLS (Fig. 3). Neither cry peptide nor cryS96 changed hydrophobicity in response to temperature changes.

The TEM, DLS and Bis-ANS results raised the question as to how the assembly influenced cry's activity as a molecular chaperone both *in vitro* and in the crowded cellular environment. We thus explored the thermodynamic mechanism underlying cryELPs' inhibition of ADH aggregation using differential scanning calorimetry (Fig. 4C). For protein systems, either a decrease in enthalpy decrease or an increase in entropy is beneficial for maintaining stability. Although no direct studies have focused on the thermodynamic mechanism underlying sHSPs' chaperone activity towards ADH, several studies suggest that stabilization of client proteins by sHSPs is dominated by enthalpic changes [37, 40]. The enthalpy increase of both plain ELPs [41] and ADH when heated indicated that both the phase transition and aggregation are endothermic processes (data not shown). Most notable at equal mass, cryS96 significantly reduced the enthalpy of ADH aggregation ($p<0.05$) (Fig. 4C), while S96 did not exhibit any effect. Remarkably, the RPE cell uptake result

corroborated our interpretation of the *in vitro* chaperone function (Fig. 6). Without oxidative stress, crystallin ELP fusions do not translocate into the nucleus. However, when oxidative stress was applied, the highest uptake was observed for crySI (large nanoparticles), followed by cryS96 (soluble macromolecule), followed by the SI ELP (small nanoparticles) lacking the αB-crystallin minipeptide. This suggests that besides cry peptide, the nanoparticle size can also influence cellular internalization in response to oxidative stress [42-44]. Based on the summary of these findings, we have proposed the mechanism for intracellular trafficking of cry96 under H_2O_2 stress (Supplementary Fig. S5).

Oxygen radicals that damage the sensitive cells in the retina are known to play a central role in the causes of AMD [45]. We and others have reported that the expression of αB-crystallin was increased with mild oxidative stress but decreased when H_2O_2 level reached a pharmacologically toxic dose [46, 47]. Moreover, our studies suggested secretion of αB-crystallin from RPE cells involved participation of exosomes [3]. The same cell model was used in this study to evaluate the *in vitro* interaction of exogenous cry ELP fusion proteins. Interestingly, the constructs have similar anti-apoptotic effects on human RPE cells under H_2O_2 stress (Fig. 5). Unexpectedly, oxidative stress in these primary cells initiated a striking level of translocation from the cell-surface and cytoplasm into the nucleus (Fig. 6), which roughly correlated with anti-apoptotic activity (Fig. 7). To the best of our knowledge, the nuclear translocation of a nanoparticle in response oxidative stress in RPE has not been observed. Once internalized, these protein polymer fusions would have direct access to misfolding client proteins inside the cytosol and the nucleus. Jeong and coworkers have previously reported that αB-crystallin physically interacts with caspase subtypes in the nucleus, which protects RPE from apoptosis [48]. Similarly, Dastoor and coworkers reported that endogenous heat shock cognate protein70 (Hsc70) translocates from the cytoplasm to the nucleus when oxidative stress is applied [49]. We have similarly reported the translocation of fluorescein labeled human recombinant αB-crystallin into the nucleus when compared with unstressed cells [3].

This manuscript shows that both cryS96 and cry escape from the endosome-lysosome degradation pathway and reach the nucleus (Fig. 8). CryS96 shows less colocalization with LAMP1 and faster trafficking to the nucleus. Del Pozo-Rodríguez and coworkers have shown that in ARPE-19 cells, inclusion of proline rich Sweet Arrow Peptide (SAP) in a delivery vesicle induced a change from clathrin dominant endocytosis to caveolae/raft-dependent endocytosis, thereby decreasing lysosomal degradation of DNA vectors [50]. Similarly, Fernández-Carneado et al. addressed the importance of proline-rich peptides in facilitating lysosomal escape as potential peptide carriers [51]. Both of these studies utilized fusion with the endosomal membrane as vesicle escape mechanism [52]. It is thus possible that the high proline content in S96, $(VPGSG)_{96}$, protected cryS96 from lysosomal attack; however, more detailed intracellular trafficking mechanisms remain to be investigated.

One of the most effective drug delivery routes for treating dry AMD is direct intravitreal administration, which is a skilled outpatient procedure associated with risks and noncompliance [53]. Extended release may reduce risks and costs by reducing the frequency of procedures [53, 54]. Biodegradable polymeric macromolecules may form a local depot in the vitreous capsule and extend their effect over longer periods [55]. The ELP system has

been proposed as a potential platform for controlled release with orthopedic applications [56], diabetes [57] and cancer treatment [58]. With this in mind, this manuscript describes the creation of new ELP nanoparticles/macromolecules with chaperone activity and potential applications in the treatment of AMD and thus may have wider applications for other therapeutic approaches in the eye.

5 Conclusion

This manuscript reports the modification of a chaperone peptide via fusion with two protein polymers, one of which assembles polymeric micelles. Unlike full-length chaperone proteins, the polymers are decorated with a sHSPs 'mini-peptide' that gives them chaperone and anti-apoptotic activity in human RPE cells. Unlike control ELPs, both crySI and cryS96 exhibit comparable anti-apoptotic activity in a model of human RPE cells, which are used to study the pathophysiology of AMD. ELP fusion modulated the assembly process, chaperone activity and intracellular uptake pathway of the native cry peptide. These findings point to the potential for intravitreal administration of these nanoparticles/macromolecules to treat AMD; however, a more detailed understanding of the mechanism underpinning oxidative stress induced nuclear translocation and *in vivo* evaluation will now be required to assess the likelihood of clinical benefit.

Supplementary Material

Refer to Web version on PubMed Central for supplementary material.

Acknowledgments

Abbreviations

cry	mini-αB-Crystallin
ELPs	Elastin like polypeptides
CMT	critical micelle temperature
ITC	inverse transition cycling
DLS	dynamic light scattering
T_t	transition temperature
R_h	hydrodynamic radius
ADH	alcohol dehydrogenase
RPE	retinal pigment epithelial

sHSPs small heat shock proteins

MDC Monodansylcadaverine

References

1. Haslbeck M, Franzmann T, Weinfurtner D, Buchner J. Some like it hot: the structure and function of small heat-shock proteins. Nature Structural & Molecular Biology. 2005; 12:842–846.

2. Arrigo AP, Simon S, Gibert B, Kretz-Remy C, Nivon M, Czekalla A, Guillet D, Moulin M, Diaz-Latoud C, Vicart P. Hsp27 (HspB1) and alphaB-crystallin (HspB5) as therapeutic targets. FEBS Lett. 2007; 581:3665–3674. [PubMed: 17467701]

3. Sreekumar PG, Kannan R, Kitamura M, Spee C, Barron E, Ryan SJ, Hinton DR. alpha B Crystallin Is Apically Secreted within Exosomes by Polarized Human Retinal Pigment Epithelium and Provides Neuroprotection to Adjacent Cells. Plos One. 2010; 5:e12578. [PubMed: 20949024]

4. De S, Rabin DM, Salero E, Lederman PL, Temple S, Stern JH. Human retinal pigment epithelium cell changes and expression of alphaB-crystallin: a biomarker for retinal pigment epithelium cell change in age-related macular degeneration. Arch Ophthalmol. 2007; 125:641–645. [PubMed: 17502503]

5. Kannan R, Sreekumar PG, Hinton DR. Novel roles for alpha-crystallins in retinal function and disease. Prog Retin Eye Res. 2012; 31:576–604. [PubMed: 22721717]

6. Kampinga HH, Hageman J, Vos MJ, Kubota H, Tanguay RM, Bruford EA, Cheetham ME, Chen B, Hightower LE. Guidelines for the nomenclature of the human heat shock proteins. Cell Stress Chaperones. 2009; 14:105–111. [PubMed: 18663603]

7. Bhattacharyya J, Padmanabha Udupa EG, Wang J, Sharma KK. Mini-alphaB-crystallin: a functional element of alphaB-crystallin with chaperone-like activity. Biochemistry. 2006; 45:3069–3076. [PubMed: 16503662]

8. Laganowsky A, Liu C, Sawaya MR, Whitelegge JP, Park J, Zhao ML, Pensalfini A, Soriaga AB, Landau M, Teng PK, Cascio D, Glabe C, Eisenberg D. Atomic View of a Toxic Amyloid Small Oligomer. Science. 2012; 335:1228–1231. [PubMed: 22403391]

9. Stengel F, Baldwin AJ, Painter AJ, Jaya N, Basha E, Kay LE, Vierling E, Robinson CV, Benesch JL. Quaternary dynamics and plasticity underlie small heat shock protein chaperone function. Proceedings of the National Academy of Sciences of the United States of America. 2010; 107:2007–2012. [PubMed: 20133845]

10. Urtti A. Challenges and obstacles of ocular pharmacokinetics and drug delivery. Advanced drug delivery reviews. 2006; 58:1131–1135. [PubMed: 17097758]

11. Vadlapudi AD, Mitra AK. Nanomicelles: an emerging platform for drug delivery to the eye. Therapeutic delivery. 2013; 4:1–3. [PubMed: 23323774]

12. Kim H, Csaky KG. Nanoparticle-integrin antagonist C16Y peptide treatment of choroidal neovascularization in rats. Journal of controlled release : official journal of the Controlled Release Society. 2010; 142:286–293. [PubMed: 19895863]

13. Zheng Y, Gu Q, Xu X. Inhibition of ocular neovascularization by a novel peptide derived from human placenta growth factor-1. Acta ophthalmologica. 2012; 90:e512–523. [PubMed: 22994140]

14. Stuart MA, Huck WT, Genzer J, Muller M, Ober C, Stamm M, Sukhorukov GB, Szleifer I, Tsukruk VV, Urban M, Winnik F, Zauscher S, Luzinov I, Minko S. Emerging applications of stimuli-responsive polymer materials. Nature materials. 2010; 9:101–113.

15. Kost J, Langer R. Responsive polymeric delivery systems. Advanced drug delivery reviews. 2001; 46:125–148. [PubMed: 11259837]

16. Fleige E, Quadir MA, Haag R. Stimuli-responsive polymeric nanocarriers for the controlled transport of active compounds: concepts and applications. Advanced drug delivery reviews. 2012; 64:866–884. [PubMed: 22349241]

17. Yang YY, Chung TS, Ng NP. Morphology, drug distribution, and in vitro release profiles of biodegradable polymeric microspheres containing protein fabricated by double-emulsion solvent extraction/evaporation method. Biomaterials. 2001; 22:231–241. [PubMed: 11197498]

18. MacEwan SR, Chilkoti A. Elastin-Like Polypeptides: Biomedical Applications of Tunable Biopolymers. Biopolymers. 2010; 94:60–77. [PubMed: 20091871]

19. Dreher MR, Simnick AJ, Fischer K, Smith RJ, Patel A, Schmidt M, Chilkoti A. Temperature triggered self-assembly of polypeptides into multivalent spherical micelles. Journal of the American Chemical Society. 2008; 130:687–694. [PubMed: 18085778]

20. Janib SM, Liu S, Park R, Pastuszka MK, Shi P, Moses AS, Orosco MM, Lin YA, Cui H, Conti PS, Li Z, MacKay JA. Kinetic quantification of protein polymer nanoparticles using noninvasive imaging. Integr Biol-UK. 2013; 5:183–194.

21. Liu W, MacKay JA, Dreher MR, Chen M, McDaniel JR, Simnick AJ, Callahan DJ, Zalutsky MR, Chilkoti A. Injectable intratumoral depot of thermally responsive polypeptide-radionuclide conjugates delays tumor progression in a mouse model. Journal of controlled release : official journal of the Controlled Release Society. 2010; 144:2–9. [PubMed: 20117157]

22. Sonoda S, Spee C, Barron E, Ryan SJ, Kannan R, Hinton DR. A protocol for the culture and differentiation of highly polarized human retinal pigment epithelial cells. Nature protocols. 2009; 4:662–673.

23. Hassouneh W, Christensen T, Chilkoti A. Elastin-like polypeptides as a purification tag for recombinant proteins. Curr Protoc Protein Sci. 2010 Chapter 6. Unit 6 11.

24. Sun G, Hsueh PY, Janib SM, Hamm-Alvarez S, MacKay JA. Design and cellular internalization of genetically engineered polypeptide nanoparticles displaying adenovirus knob domain. Journal of controlled release : official journal of the Controlled Release Society. 2011; 155:218–226. [PubMed: 21699930]

25. Shah M, Edman MC, Janga SR, Shi P, Dhandhukia J, Liu SY, Louie SG, Rodgers K, MacKay JA, Hamm-Alvarez SF. A rapamycin-binding protein polymer nanoparticle shows potent therapeutic activity in suppressing autoimmune dacryoadenitis in a mouse model of Sjogren's syndrome. Journal of controlled release : official journal of the Controlled Release Society. 2013; 171:269–279. [PubMed: 23892265]

26. Sreekumar PG, Chothe P, Sharma KK, Baid R, Kompella U, Spee C, Kannan N, Manh C, Ryan SJ, Ganapathy V, Kannan R, Hinton DR. Antiapoptotic properties of alpha-crystallin-derived peptide chaperones and characterization of their uptake transporters in human RPE cells. Invest Ophthalmol Vis Sci. 2013; 54:2787–2798. [PubMed: 23532520]

27. Augood CA, Vingerling JR, de Jong PT, Chakravarthy U, Seland J, Soubrane G, Tomazzoli L, Topouzis F, Bentham G, Rahu M, Vioque J, Young IS, Fletcher AE. Prevalence of age-related maculopathy in older Europeans: the European Eye Study (EUREYE). Archives of ophthalmology. 2006; 124:529–535. [PubMed: 16606879]

28. Neef DW, Jaeger AM, Thiele DJ. Heat shock transcription factor 1 as a therapeutic target in neurodegenerative diseases. Nat Rev Drug Discov. 2011; 10:930–944. [PubMed: 22129991]

29. McClellan AJ, Tam S, Kaganovich D, Frydman J. Protein quality control: chaperones culling corrupt conformations. Nature cell biology. 2005; 7:736–741.

30. Morimoto RI, Santoro MG. Stress-inducible responses and heat shock proteins: new pharmacologic targets for cytoprotection. Nature biotechnology. 1998; 16:833–838.

31. Mymrikov EV, Seit-Nebi AS, Gusev NB. Large potentials of small heat shock proteins. Physiological reviews. 2011; 91:1123–1159. [PubMed: 22013208]

32. Ousman SS, Tomooka BH, van Noort JM, Wawrousek EF, O'Connor KC, Hafler DA, Sobel RA, Robinson WH, Steinman L. Protective and therapeutic role for alphaB-crystallin in autoimmune demyelination. Nature. 2007; 448:474–479. [PubMed: 17568699]

33. Rothbard JB, Kurnellas MP, Brownell S, Adams CM, Su L, Axtell RC, Chen R, Fathman CG, Robinson WH, Steinman L. Therapeutic effects of systemic administration of chaperone alphaB-crystallin associated with binding proinflammatory plasma proteins. The Journal of biological chemistry. 2012; 287:9708–9721. [PubMed: 22308023]

34. Arac A, Brownell SE, Rothbard JB, Chen C, Ko RM, Pereira MP, Albers GW, Steinman L, Steinberg GK. Systemic augmentation of alphaB-crystallin provides therapeutic benefit twelve hours post-stroke onset via immune modulation. Proceedings of the National Academy of Sciences of the United States of America. 2011; 108:13287–13292. [PubMed: 21828004]

35. Mornon JP, Halaby D, Malfois M, Durand P, Callebaut I, Tardieu A. alpha-crystallin C-terminal domain: on the track of an Ig fold. Int J Biol Macromol. 1998; 22:219–227. [PubMed: 9650076]

36. Knowles TP, Fitzpatrick AW, Meehan S, Mott HR, Vendruscolo M, Dobson CM, Welland ME. Role of intermolecular forces in defining material properties of protein nanofibrils. Science. 2007; 318:1900–1903. [PubMed: 18096801]

37. Kumar MS, Kapoor M, Sinha S, Reddy GB. Insights into hydrophobicity and the chaperone-like function of alpha A- and alpha B-crystallins. J Biol Chem. 2005; 280:21726–21730. [PubMed: 15817465]

38. Reddy GB, Kumar PA, Kumar MS. Chaperone-like activity and hydrophobicity of alpha-crystallin. IUBMB life. 2006; 58:632–641. [PubMed: 17085382]

39. McHaourab HS, Godar JA, Stewart PL. Structure and mechanism of protein stability sensors: chaperone activity of small heat shock proteins. Biochemistry. 2009; 48:3828–3837. [PubMed: 19323523]

40. Kazlauskas E, Petrikaite V, Michailoviene V, Revuckiene J, Matuliene J, Grinius L, Matulis D. Thermodynamics of aryl-dihydroxyphenyl-thiadiazole binding to human Hsp90. Plos One. 2012; 7:e36899. [PubMed: 22655030]

41. Urry DW. Physical chemistry of biological free energy transduction as demonstrated by elastic protein-based polymers. J Phys Chem B. 1997; 101:11007–11028.

42. Nel AE, Madler L, Velegol D, Xia T, Hoek EMV, Somasundaran P, Klaessig F, Castranova V, Thompson M. Understanding biophysicochemical interactions at the nano-bio interface. Nat Mater. 2009; 8:543–557. [PubMed: 19525947]

43. Petros RA, DeSimone JM. Strategies in the design of nanoparticles for therapeutic applications. Nat Rev Drug Discov. 2010; 9:615–627. [PubMed: 20616808]

44. Geng Y, Dalhaimer P, Cai SS, Tsai R, Tewari M, Minko T, Discher DE. Shape effects of filaments versus spherical particles in flow and drug delivery. Nat Nanotechnol. 2007; 2:249–255. [PubMed: 18654271]

45. Sanvicens N, Gomez-Vicente V, Masip I, Messeguer A, Cotter TG. Oxidative stress-induced apoptosis in retinal photoreceptor cells is mediated by calpains and caspases and blocked by the oxygen radical scavenger CR-6. Journal of Biological Chemistry. 2004; 279:39268–39278. [PubMed: 15210718]

46. Shin JH, Kim SW, Lim CM, Jeong JY, Piao CS, Lee JK. alpha B-crystallin suppresses oxidative stress-induced astrocyte apoptosis by inhibiting caspase-3 activation. Neurosci Res. 2009; 64:355–361. [PubMed: 19379782]

47. Yaung J, Jin ML, Barron E, Spee C, Wawrousek EF, Kannan R, Hinton DR. alpha-Crystallin distribution in retinal pigment epithelium and effect of gene knockouts on sensitivity to oxidative stress. Mol Vis. 2007; 13:566–577. [PubMed: 17438522]

48. Jeong WJ, Rho JH, Yoon YG, Yoo SH, Jeong NY, Ryu WY, Ahn HB, Park WC, Rho SH, Yoon HS, Choi YH, Yoo YH. Cytoplasmic and nuclear anti-apoptotic roles of alphaB-crystallin in retinal pigment epithelial cells. Plos One. 2012; 7:e45754. [PubMed: 23049853]

49. Dastoor Z, Dreyer JL. Nuclear translocation and aggregate formation of heat shock cognate protein 70 (Hsc70) in oxidative stress and apoptosis. J Cell Sci. 2000; 113:2845–2854. [PubMed: 10910769]

50. del Pozo-Rodriguez A, Pujals S, Delgado D, Solinis MA, Gascon AR, Giralt E, Pedraz JL. A proline-rich peptide improves cell transfection of solid lipid nanoparticle-based non-viral vectors. Journal of controlled release : official journal of the Controlled Release Society. 2009; 133:52–59. [PubMed: 18854203]

51. Fernandez-Carneado J, Kogan MJ, Castel S, Giralt E. Potential peptide carriers: amphipathic proline-rich peptides derived from the N-terminal domain of gamma-zein. Angew Chem Int Ed Engl. 2004; 43:1811–1814. [PubMed: 15054781]

52. Varkouhi AK, Scholte M, Storm G, Haisma HJ. Endosomal escape pathways for delivery of biologicals. Journal of controlled release : official journal of the Controlled Release Society. 2011; 151:220–228. [PubMed: 21078351]

53. Evans JB, Syed BA. New hope for dry AMD?, Nature reviews. Drug discovery. 2013; 12:501–502. [PubMed: 23812264]

54. Garber K. Biotech in a blink. Nature biotechnology. 2010; 28:311–314.

55. Nagarwal RC, Kant S, Singh PN, Maiti P, Pandit JK. Polymeric nanoparticulate system: a potential approach for ocular drug delivery. Journal of controlled release : official journal of the Controlled Release Society. 2009; 136:2–13. [PubMed: 19331856]

56. Adams SB Jr. Shamji MF, Nettles DL, Hwang P, Setton LA. Sustained release of antibiotics from injectable and thermally responsive polypeptide depots. Journal of biomedical materials research. Part B, Applied biomaterials. 2009; 90:67–74.

57. Amiram M, Luginbuhl KM, Li X, Feinglos MN, Chilkoti A. A depot-forming glucagon-like peptide-1 fusion protein reduces blood glucose for five days with a single injection. Journal of controlled release : official journal of the Controlled Release Society. 2013; 172:144–151. [PubMed: 23928357]

58. Liu W, Dreher MR, Furgeson DY, Peixoto KV, Yuan H, Zalutsky MR, Chilkoti A. Tumor accumulation, degradation and pharmacokinetics of elastin-like polypeptides in nude mice. Journal of controlled release : official journal of the Controlled Release Society. 2006; 116:170–178. [PubMed: 16919353]
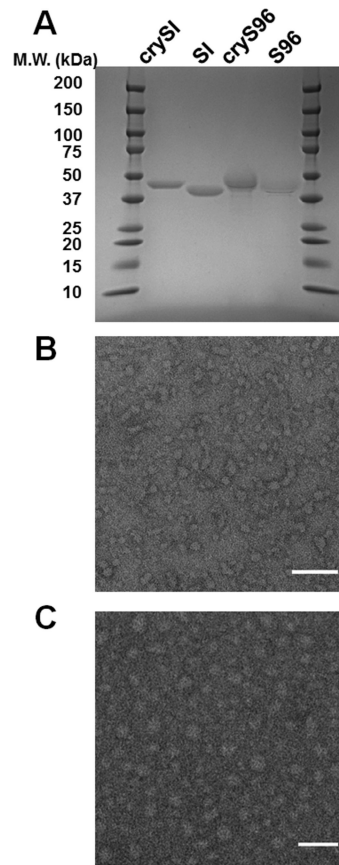
**Figure 1. Purity of ELP fusions and morphology of protein polymer nanoparticles**
A) SDS-PAGE was used to characterize the purity and molecular weight for ELP fusion proteins (Table 1), which were stained using Coomassie blue. The molecular weight for the ladder is indicated to the left. **B**) TEM image of SI nanoparticles, with average diameters of 29.1 ± 3.4nm. **C**) TEM image of crySI nanoparticles, with average diameters of 28.7 ± 6.2nm. Scale bar: 100nm.
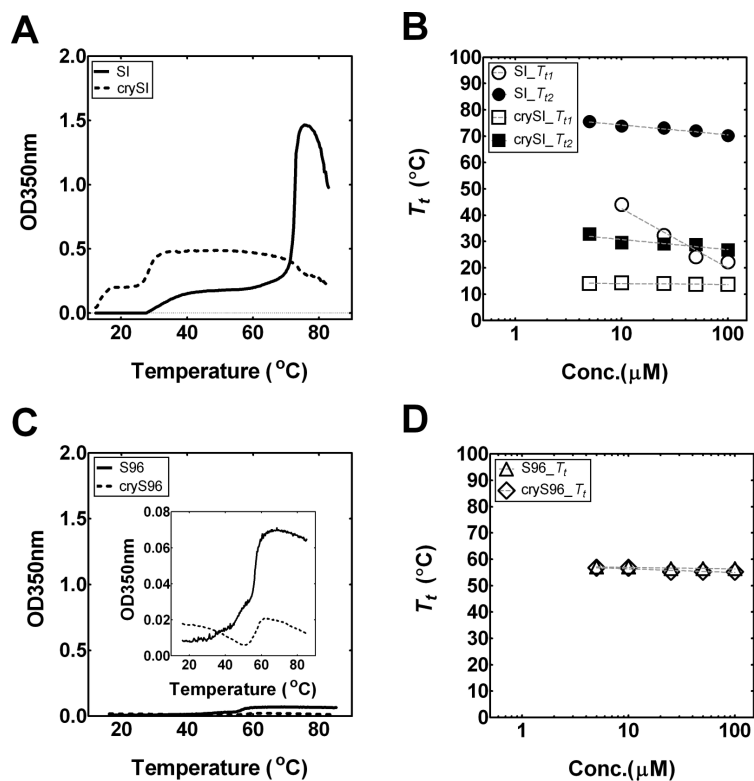
Figure 2. Phase diagrams for mono and diblock ELP fusion proteins

Optical density (OD_{350} nm) was used to monitor temperature-dependent assembly of ELPs. **A**) The SI and crySI diblocks (25 μM) undergo two obvious phase transitions. T_{t1} is associated with phase separation of the hydrophobic ELP (Xaa=Ile), which drives nanoparticle assembly. Occurring at a higher temperature, T_{t2} is attributed to bulk phase separation into larger nanostructures. For SI, T_{t1} and T_{t2} are 26 and 70 °C respectively. Similarly, for crySI, T_{t1} and T_{t2} are 12 and 30 °C respectively. **B**) Concentration-temperature phase diagrams for SI and crySI diblock copolymers. **C**) In contrast, the monoblocks protein polymers S96 and cryS96 (25 μM) demonstrate only one phase separation near 56°C. **D**) Concentration-temperature phase diagram for S96 and cryS96. Dashed lines indicate the fit of T_t to the following equation $T_t = m\log[\text{ELP}] + b$ where [ELP] is the concentration, m is the slope, and b is the transition temperature at 1 μM.
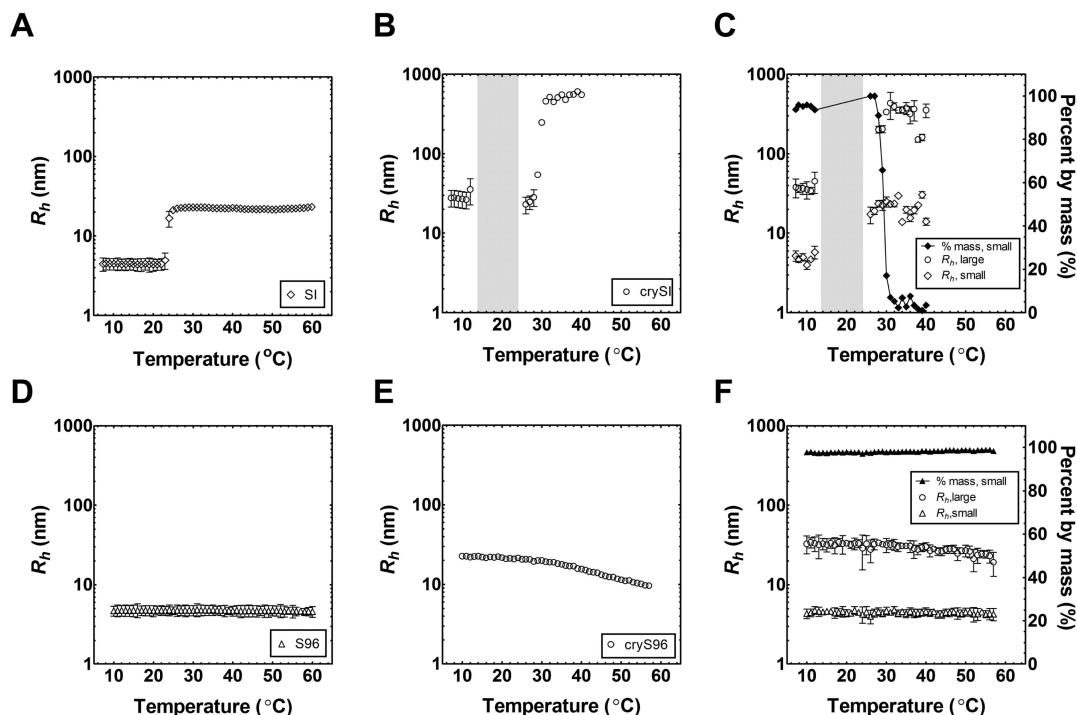
Figure 3. The αB-crystallin mini-peptide influences the assembly and radius of ELP nanoparticles

The particle hydrodynamic radius (R_h) was measured (25 μM) as a function of temperature using dynamic light scattering. Panels **A**,**B**,**D**,**E** represent the cumulant fit, which reflects the particle population that scatters the most light. Panels **C**,**F** represent a regularization fit, which can separate populations of particles with different size. **A**) SI diblocks form monodisperse nanoparticles above their critical micelle temperature (26 °C) that remain stable at physiologic temperatures (37 °C). **B**) In contrast, crySI shows an increased radius even at the lowest assayed temperature (7 °C). Extended autocorrelation times were observed in the indicated grey region that prevented the estimation of hydrodynamic radius using standard models. Above 30 °C, crySI forms ~400nm nanoparticles. **C**) Regularization analysis enabled two populations of particles to be observed for crySI. Below 30 °C the dominant popula tion of small particles behaved like SI, which accounted for about 95 % of the sample by mass. Above 30 °C a population of larger particles dominated the sample. **D**) S96 remains monomeric over 10 to 60 °C. **E**) In contrast, cryS96 has a larger radius than S96 over the entire temperature range. **F**) Regularization analysis enabled the observation of two populations of particles in the sample of cryS96. The dominant species for cryS96 has a radius similar to monomeric S96, which represented about 95 % of the sample by mass.
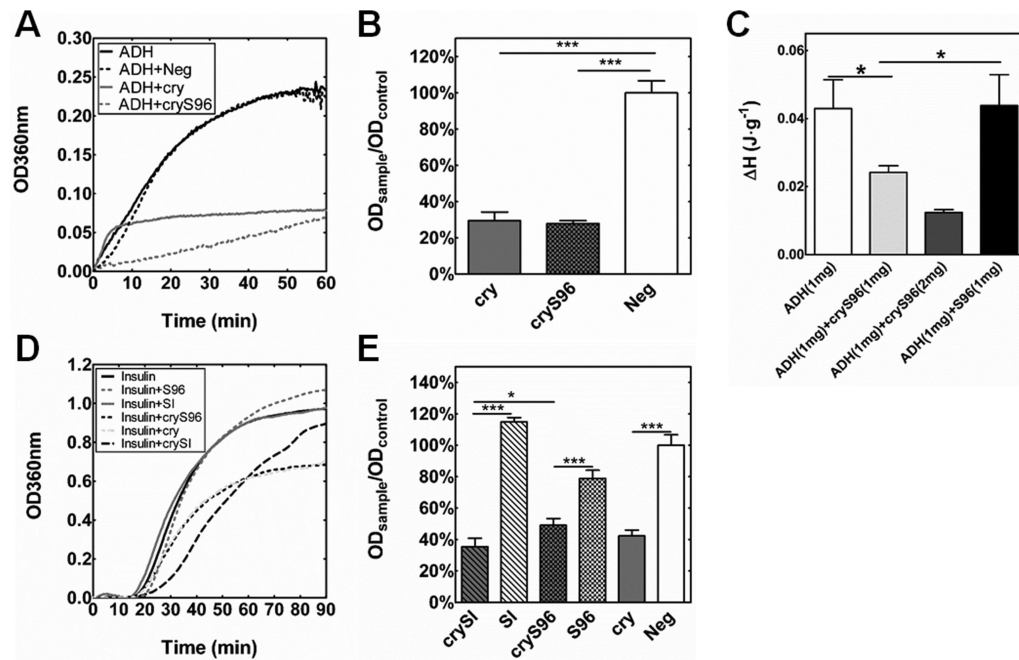
Figure 4. ELP fusion proteins have protective chaperone activity on ADH and insulin
A) Representative chaperone activity of cryS96 and mini-peptide alone (cry) against heat
induced ADH aggregation at 48 °C. **B**) Both reduced (p<0.001) the onset of turbidity
compared to a scrambled mini-peptide (Neg) at 1h (500 μM). **C**) DSC measurement of H
change at 48 °C showing cryS96 reduced the aggregation enthalpy per mass of ADH in a
dose dependent manner. (*p<0.05). **D**) An insulin aggregation assay confirmed the
chaperone activity of the ELP fusions with the mini-peptide (100 μM) at 12 °C. Both cryS96
and crySI protect ag ainst DTT induced aggregation, while unmodified S96 and SI did not.
E) A quantitative comparison of insulin aggregation in the presence of ELPs at 30 min.
crySI and cryS96 significantly (p<0.001) inhibited aggregation compared to SI and S96
respectively. Data indicate mean+S.D. (n=3), which were analyzed using one-way ANOVA.
(***p<0.001).
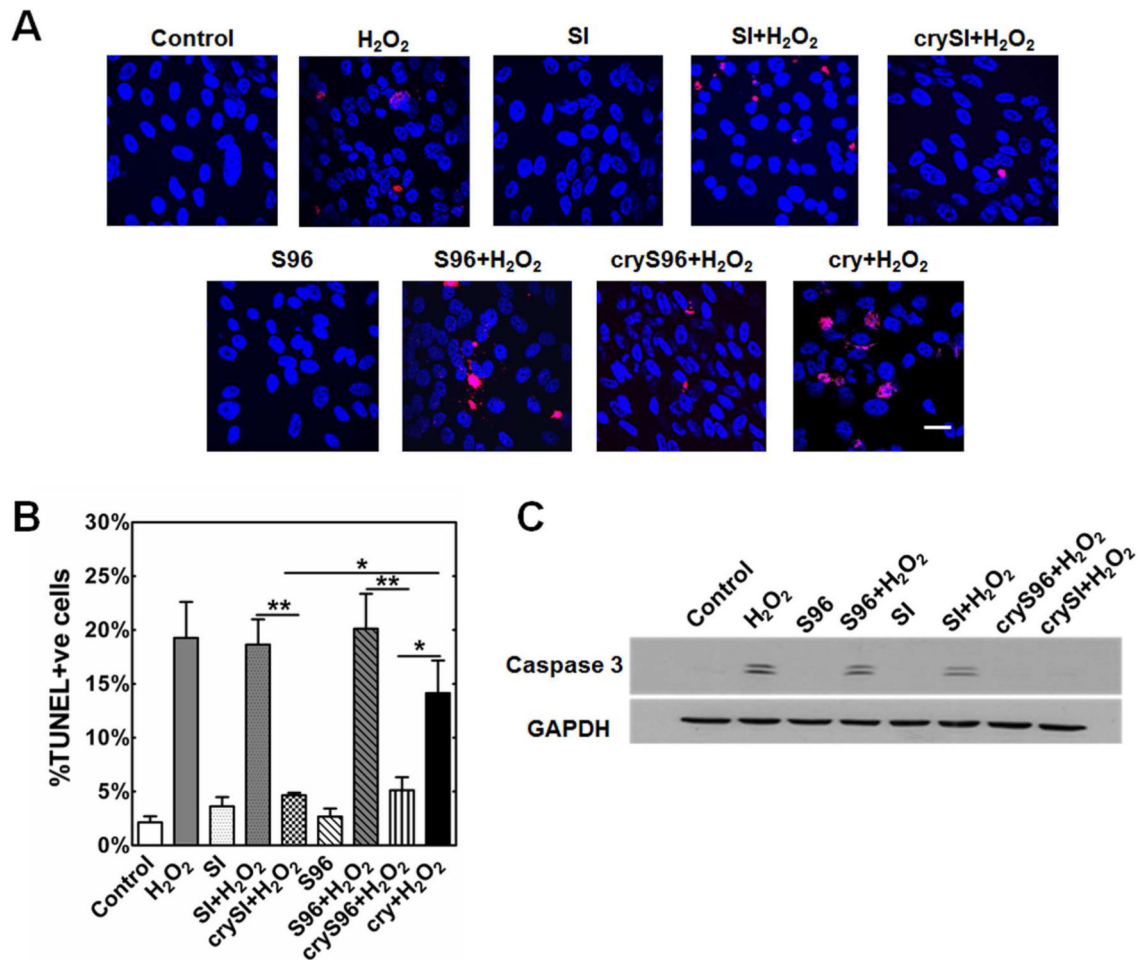
Figure 5. ELP fusion proteins protect RPE cells from H_2O_2 induced cell death
Human RPE cells were treated with 200 μM H_2O_2 for 24h with or without crySI or cryS96. Cell death was assessed by the TUNEL assay and activation of cleaved caspase-3 by immunoblot analysis. **A**) TUNEL assay showing co-treatment of H_2O_2 and unmodified ELPs did not inhibit apoptosis in RPE cells whereas crySI and cryS96 significantly reduced cell death. Confocal images of TUNEL-positive cells (red) and nuclei (blue) are shown. **B**) Quantification of TUNEL-positive cells. Data are presented as percent of TUNEL-positive cells. (*p<0.05, **p<0.01) **C**) Representative western blot showing exogenous crySI and cryS96 protected RPE cells from oxidative stress by inhibiting activation of caspase-3. Caspase-3 activation was prominent in control cells treated with 200 μM H_2O_2. Unmodified ELPs SI and S96 failed to protect against caspase-3 activation. Scale bar: 20 μm.
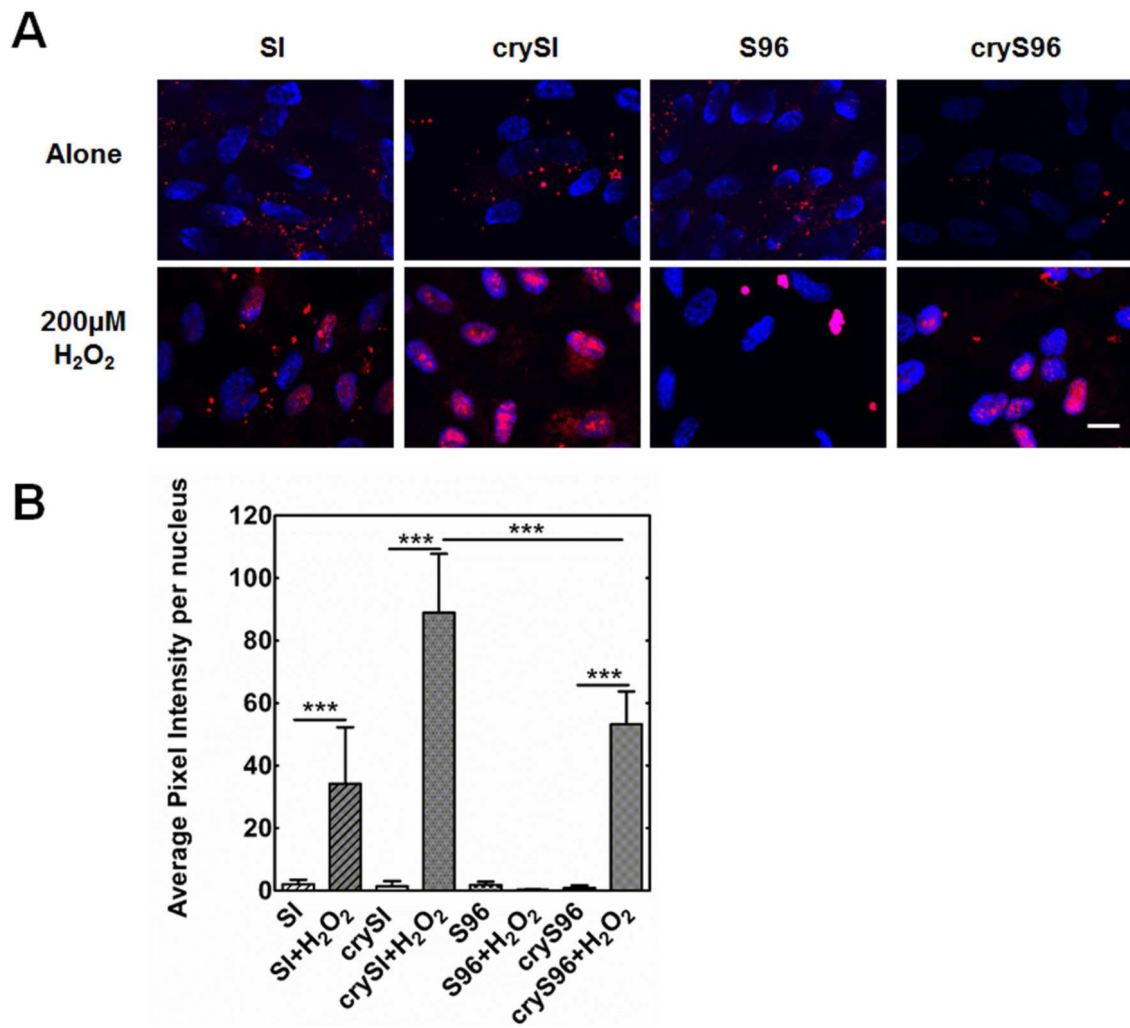
Figure 6. Uptake and nuclear translocation of exogenous ELPs in RPE cells
A) RPE cells were starved in serum free medium and treated with either 5 M rhodamine labeled ELPs alone or co-treated with 200 M H_2O_2 for 24h. Oxidative stress induced nuclear uptake of labeled crySI and cryS96. **B**) Quantification of RPE cell uptake of ELPs. Both crySI and cryS96 exhibited significantly enhanced nuclear uptake level under H_2O_2 stress compared to ELP control groups (***$p < 0.001$). Uptake level of crySI nanoparticles was higher than cryS96 (***$p < 0.001$). Scale bar: 20 μm.
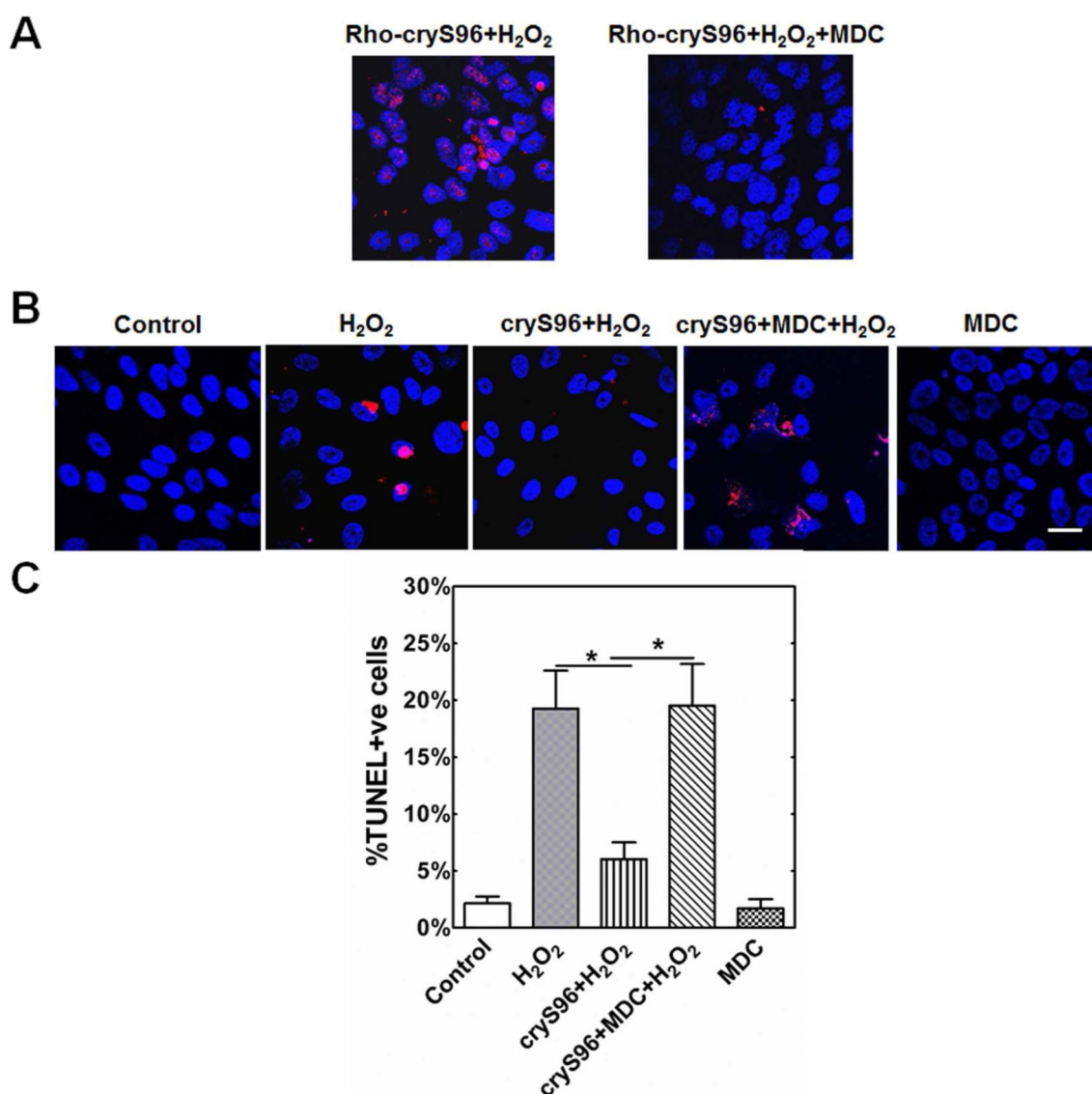
Figure 7. Uptake and nuclear translocation plays an important role in cryS96's anti-apoptotic activity

Cells were pre-incubated with 100 μM MDC for 30 min followed by co-incubation with 5 μM rhodamine labeled cryS96 for 24 h along with 200 μM H_2O_2. Control cells represent no treatment with either MDC or H_2O_2. **A**) Representative confocal images of cell uptake showing MDC can inhibit cell uptake of exogenous cryS96. Red: rhodamine labeled cryS96; Blue: DAPI. **B**) Representative TUNEL images showing MDC significantly (*p<0.05) reduced the anti-apoptosis efficacy of cryS96 under H_2O_2 stress. Red: TUNEL+ cells (apoptosis), Blue: DAPI. **C**) Quantification of TUNEL positive cells from B). (*p<0.05). Scale bar: 20 μm.
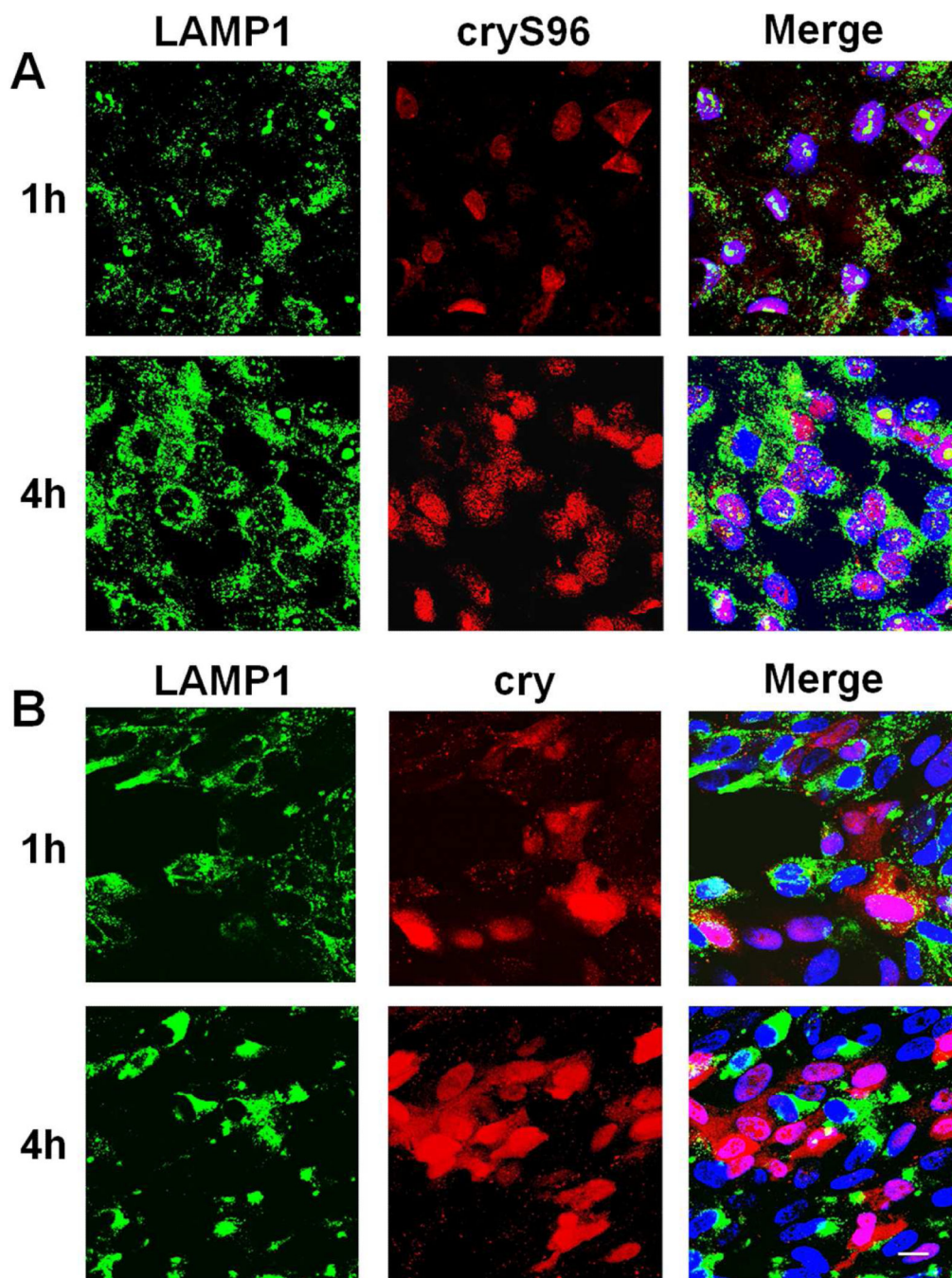
Figure 8. Intracellular trafficking of cryS96 and cry peptide under H_2O_2 stress
A)Representative images showing time dependent nuclear translocation of cryS96 (red) under H_2O_2 stress in human RPE cells. **B**) Intracellular trafficking of the free cry peptide (red) under same condition. Red: fluorescence; Green: LAMP1; Blue: DAPI. Scale bar: 20 µm.

Table 1

Nomenclature, sequence and molecular weight of ELP fusion proteins

Peptide label	Amino Acid Sequence	*Expected M.W. (kDa)	**Observed M.W. (kDa)
SI	G(VPGSG)$_{48}$(VPGIG)$_{48}$Y	39.65	39.54
crySI	GDRFSVNLDVKHFSPEELKVKG(VPGSG)$_{48}$(VPGIG)$_{48}$Y	42.07	42.06
S96	G(VPGSG)$_{96}$Y	38.39	38.22
cryS96	GDRFSVNLDVKHFSPEELKVKG(VPGSG)$_{96}$Y	40.82	40.72

*Expected M.W.(m/z) was calculated by DNAStar Lasergene Editseq excluding the methionine start codon

**Observed M.W. ([M+H]$^{+}$) was measured by MALDI-TOF